Electrostatic Guidance of Glycosyl Cation Migration along the Reaction Coordinate of Uracil DNA Glycosylase[†,‡]

Mario A. Bianchet,[§,||] Lauren A. Seiple,[§,⊥] Yu Lin Jiang,[⊥] Yoshitaka Ichikawa,[#] L. Mario Amzel,[||] and James T. Stivers*[,⊥]

Departments of Pharmacology and Molecular Sciences and Biophysics, The Johns Hopkins University School of Medicine, 725 North Wolfe Street, Baltimore, Maryland 21205, and Optimer Pharmaceuticals, Inc., 10130 Sorrento Valley Road, Suite D, San Diego, California 92121

Received August 1, 2003; Revised Manuscript Received September 12, 2003

ABSTRACT: The DNA repair enzyme uracil DNA glycosylase has been crystallized with a cationic 1-aza-2′-deoxyribose-containing DNA that mimics the ultimate transition state of the reaction in which the water nucleophile attacks the anomeric center of the oxacarbenium ion−uracil anion reaction intermediate. Comparison with substrate and product structures, and the previous structure of the intermediate determined by kinetic isotope effects, reveals an exquisite example of geometric strain, least atomic motion, and electrophile migration in biological catalysis. This structure provides a rare opportunity to reconstruct the detailed structural transformations that occur along an enzymatic reaction coordinate.

An essential hallmark of enzyme catalysis is the enzyme-facilitated routing of substrate and intermediates along a defined reaction coordinate that ultimately leads to enzyme-bound products. Such mechanisms are unique from nonenzymatic catalysis and require the use of directed forces and/or motions of the enzyme that selectively enforce an evolutionarily selected reaction pathway (*1*). Mechanisms of enzymatic glycosyl transfer typically involve the generation of extremely unstable glycosyl cation transition states or intermediates that require tremendous stabilization by the active site environment of enzymes (*2*); these reactions provide a fascinating opportunity to study how enzymes direct the reactivity of unstable intermediates between a departing leaving group and an attacking nucleophile.

The illumination of these mechanisms is very often elusive but is best approached using a battery of complementary techniques that are designed to reveal discrete characteristics of the reaction coordinate. Over the last 5 years the reaction mechanism of the powerful DNA repair enzyme uracil DNA glycosylase (UDG) has been systematically dissected using crystallography (*3*, *4*), heteronuclear NMR spectroscopy (*5*−*7*), Raman spectroscopy (*8*), and multiple kinetic isotope effect (KIE) measurements (*9*). Features of the catalytic mechanism include the use of ground-state strain to preorganize the deoxyuridine reactant in a distorted 3′-exo sugar pucker that facilitates electronic stabilization of a dissociative transition state and planar oxacarbenium ion intermediate (Figure 1). Stabilization of the intermediate is brought about by electrostatic interactions with the anionic uracil leaving group (*10*, *11*), an aspartate residue (Asp145) (*10*, *11*), and nearby phosphodiester groups of the DNA substrate (*12*, *13*). Then, in a second transition state, UDG promotes direct and irreversible attack of the nucleophilic water at the anomeric carbon, resulting in inversion of configuration at the anomeric center of the product (Figure 1) (*3*).

UDG is a paradigm for elucidation of structural transformations along the reaction coordinate for glycosyl transfer because high-resolution crystal structures of substrate and product complexes have been determined (*3*, *4*), and the geometry of the sugar ring in the intermediate has been determined by KIE studies (*14*). However, an unresolved issue is the structure of the second transition state in which the water nucleophile attacks the anomeric carbon. A key issue in this final step is whether the nucleophile or the electrophile migrates to bring these reacting groups together, because in the substrate and intermediate complexes these groups are not within covalent bonding distance (*15*). A unique and interesting structural requirement of the electrophile migration mechanism is that the rigid planarity of the intermediate must first be broken in order to present the electron-deficient anomeric center to the stationary water nucleophile (Figure 1).

To address this question, we have now determined the crystal structure of human UDG (hUDG) in complex with uracil and DNA containing a cationic 1-azadeoxyribose (1-aza-dR) glycosyl cation analogue (Figure 1). We have previously shown that 1-aza-dR is a potent inhibitor of UDG only when the uracil anion leaving group, Asp145, and DNA phosphates are present (K_I = 100−500 pM) (*11*, *16*) and that 1-aza-dR mimics the expected features of a high-energy transition state or intermediate on the reaction coordinate (*10*). Here we provide structural evidence that 1-aza-dR

[†] This work was supported by NIH Grants GM56834 (J.T.S.) and GM66895 (L.M.A.).

[‡] The structural coordinates for the ternary complex have been deposited in the Protein Data Bank (1Q3F).

* Address correspondence to this author. E-mail: jstivers@jhmi.edu.

[§] These authors contributed equally to this work.

[||] Department of Biophysics, The Johns Hopkins University School of Medicine.

[⊥] Department of Pharmacology and Molecular Sciences, The Johns Hopkins University School of Medicine.

[#] Optimer Pharmaceuticals, Inc.

10.1021/bi035372+ CCC: $25.00
Published on Web 10/11/2003

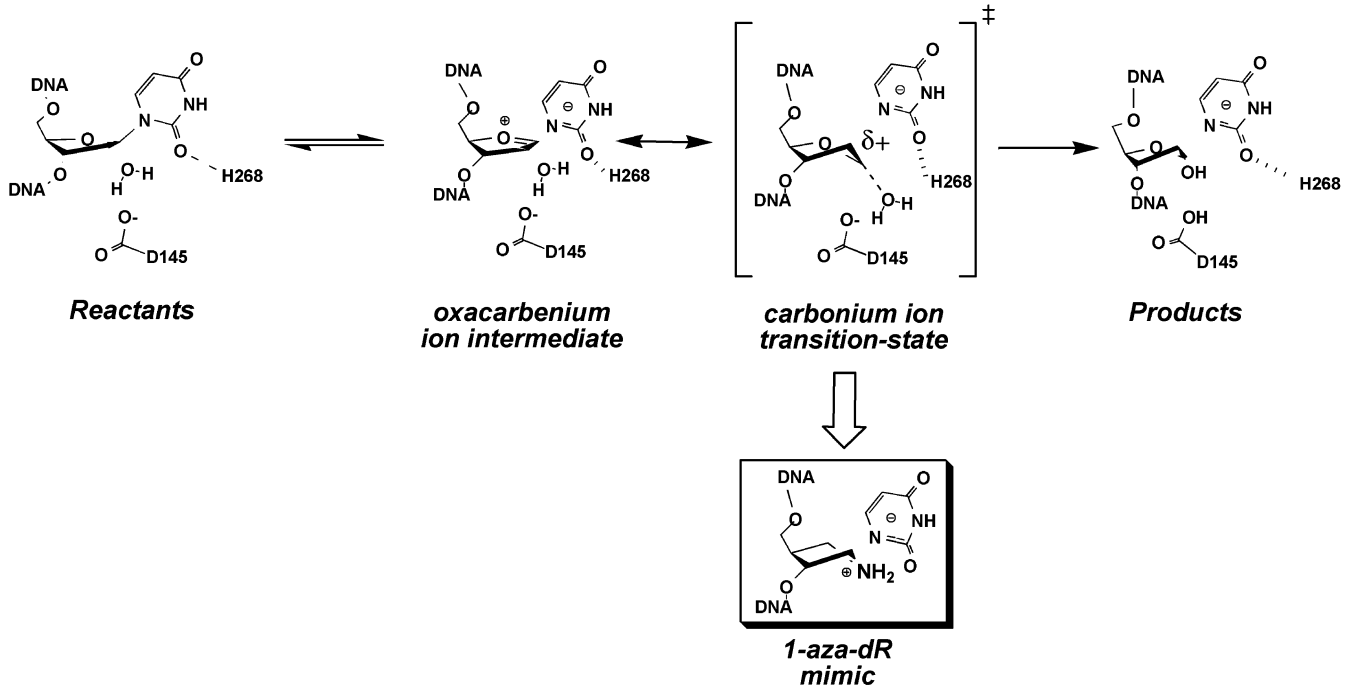

FIGURE 1: Reaction pathway of UDG. A stepwise mechanism has been established involving a discrete oxacarbenium ion intermediate that is stabilized by electrostatic interactions with active site residues and the phosphodiester groups of the DNA. Two catalytic groups are indicated in the figure: His268, which serves as a hydrogen bond donor to stabilize the developing negative charge on uracil O2 in the dissociative transition state, and Asp145, which stabilizes the cationic sugar of the intermediate. The structure of 1-aza-dR, which is proposed to mimic the sugar conformation in the second transition state involving water addition, is also shown.

adopts a conformation that mimics the final transition state in which the electrophilic sugar migrates to meet the attacking water nucleophile. This structure now allows a complete reconstruction of the reaction coordinate for this important DNA repair enzyme.

EXPERIMENTAL PROCEDURES

Cloning and Purification of Human UDG. Human UDG was amplified by PCR from a human testis cDNA library (*17*) using primers that targeted the catalytic domain comprising residues 85−304. The PCR product was isolated by gel electrophoresis, digested with restriction enzymes *Nde*I and *Hin*dIII, and inserted into the corresponding sites in the expression vector pET21a (Novagen, Madison, WI). The pET21a-hUDG construct was transformed into the BL21-CodonPlus(DE3)-RP *Escherichia coli* strain (Stratagene, La Jolla, CA). The sequence was confirmed by automated sequencing of both DNA strands.

The purification was carried out as previously described (*17*), except that Bugbuster protein extraction reagent and benzonase nuclease (Novagen, Madison, WI) were used for cell lysis and nucleic acid degradation, respectively. About 12 mg of purified protein was obtained from 2 L of bacterial cell culture. The enzyme concentration was calculated using $\epsilon^{280} = 33680\ M^{-1}\ cm^{-1}$ (6 M GuHCl), and enzyme activity was verified using a continuous kinetic assay (*18*).

Crystallization, Data Collection, Processing, and Refinement of the Ternary Complex. Crystallization was performed by hanging-drop vapor diffusion after addition of equal volumes of a preformed UDG−uracil−1-aza-dR DNA complex to a reservoir solution containing 1.5 mM dithiothreitol (DTT), 18% poly(ethylene glycol) 4000 (PEG 4000), 10% dioxane, and 100 mM HEPES, pH 6.5 (*4*). The final concentrations of hUDG, DNA, and uracil in the drop were 8.8 mg/mL, 1 mM, and 0.5 mM, respectively. The DNA sequence was 5′-TGTIATCTT-3′:3′-ACAATAGAAA-5′, where I is the 1-aza-dR residue.

Data were collected in-house on a Rigaku RU-H200 rotating anode X-ray generator with a Cu target and a Raxis IV detector. The hUDG crystal was flash frozen by plunging it in LN_2 suspended in a very thin film of mother liquor, achieved by repetitive blotting of the loop. Data reduction was performed with the programs Denzo and Scalepack (*19*). The initial model was obtained by molecular replacement using the coordinates of the native enzyme (PDB accession code 1AKZ) as the search model. Calculations were carried out with the program MOLREP from the CCP4 package (*20*). A solution with a 21% correlation (next solution 6%) was obtained using data from 36.0 to 3.0 Å. The initial difference Fourier map showed positive density that was interpreted as the bound 1-aza-2′-deoxyribose-containing DNA, as the bound uracil, and as changes in the protein associated with the binding to DNA. Rebuilding of the structure was performed in sigma A weighted maps using the modeling program O (*21*). The final model of the crystal structure including nucleotides, uracil, a single phosphate, and 275 water molecules was refined using data up to 1.9 Å resolution with the program CNS 1.1 (*22*). Figures were drawn using PyMOL (*29*).

Molecular Mechanics Calculations. The equilibrium geometry of the 1-aza-dR was calculated using the program Spartan Pro (Wavefunction, Irvine, CA) using the MMFF molecular mechanics force field. The gas-phase calculations were performed by extracting the 1-aza-dR residue and the 3′- and 5′-hydroxyl groups from the crystal model and

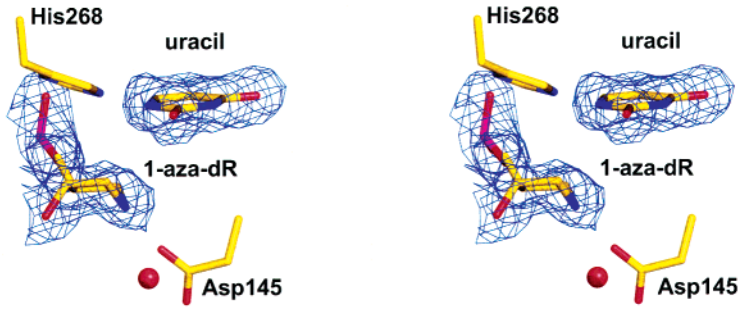

FIGURE 2: Electron density map ($2F_o - F_c$ contoured at 1σ) and structural model of the complex of human UDG with 1-aza-dR and uracil.

Table 1: Crystallographic Data Collection and Refinement Statistics

Crystallographic Data	
space group	$P2_12_12_1$
cell dimensions (Å)	$a = 48.7$, $b = 65.85$, $c = 99.5$
resolution range (Å)	36.5−1.9
R_{sym}[a]	0.06 (0.25)[b]
completeness (%)	94.9 (69.1)
multiplicity	4.7 (2.1)[b]
$I/\sigma(I)$	16.2 (2.2)[b]
no. of reflections	24682
Model Refinement	
no. of atoms [average B (Å^2)]	
protein	1808 (17.9)
solvent	275 (28.5)
ligands	388 (35.5)
total	2471 (21.8)
F data cutoff (in F units)	0
R value	0.195
R_{free} (test set of 9.2%)	0.235
bond length rms (Å)	0.0066
bond angles (deg)	1.3

[a] $R_{sym} = \sum_h\sum_j|I_{hj} - \langle I_h\rangle|/\sum_h\sum_j|I_{hj}|$, where h represents a unique reflection and j means symmetry-equivalent indices, I is the observed intensity, and $\langle I\rangle$ is the mean value of I. [b] Last shell.

allowing the atoms to relax to the energy-optimized geometry without any restraints. To investigate the role of phosphodiester backbone immobilization in determining the sugar pucker, a second geometry optimization was performed in which the C5′, C4′, C3′, and O3′ atoms were frozen and the other atoms were allowed to reach their equilibrium positions during the calculations. Similar sugar conformations were obtained using Hartree−Fock and density functional methods (not shown).

RESULTS AND DISCUSSION

Structure of the Ternary Complex of hUDG, Uracil, and 1-Aza-dR. The crystals of hUDG and a DNA duplex containing a 1-aza-dR residue were obtained in the presence of 0.5 mM uracil using similar crystallization conditions as previously reported for the complex of UDG with the *C*-glycoside substrate analogue, pseudodeoxyuridine (*4*). The crystal of the ternary complex diffracted to 1.9 Å resolution using an in-house rotating anode X-ray source, yielding an excellent electron density of the active site region (Figure 2 and Table 1). The global structure of the complex was essentially indistinguishable from the substrate and product complexes (*3*, *4*). However, a remarkable and perhaps unprecedented aspect of the current structure is the extreme distortion of the 1-azadeoxyribose sugar, which is found to be bent downward toward Asp145, likely due to a strong electrostatic attraction between the anionic carboxylate and

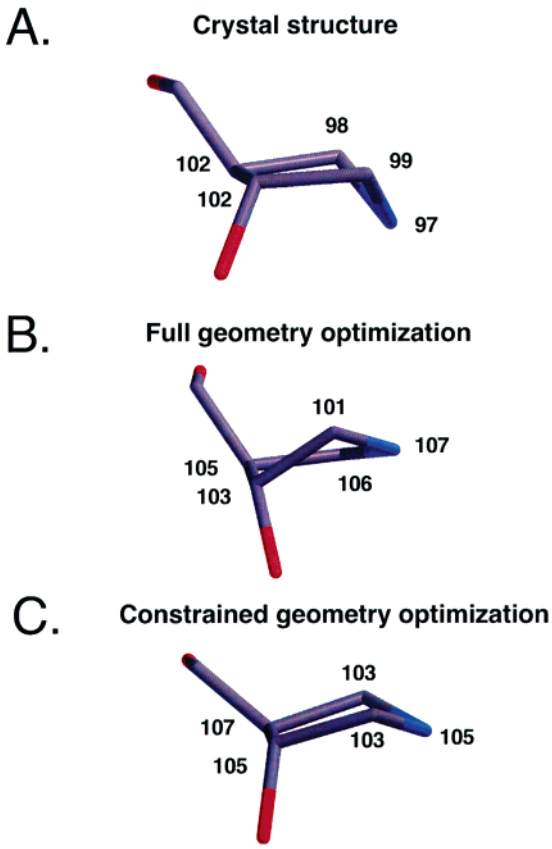

FIGURE 3: Highly distorted bond angles in the 1-aza-dR ring as compared to the MMFF geometry-optimized conformation with the endocyclic carbon bond angles indicated (see Experimental Procedures). (A) Conformation of 1-aza-dR in the UDG active site. (B) Unrestrained geometry-optimized conformation of the 1-aza-dR sugar. (C) Constrained geometry optimization in which the C5′, C4′, C3′, and O3′ atoms were frozen to mimic the rigidly positioned DNA backbone enforced by the enzyme (see text).

the cationic secondary amine of 1-aza-dR ($r = 2.9$ Å) (*11*). This bent conformation differs grossly from the essentially planar conformation of the sugar ring that is observed in the substrate analogue complex (*4*) (see also Figure 4 below) and which was also calculated for the oxacarbenium ion intermediate using the stereospecific β deuterium KIEs (*14*). Thus the tight-binding 1-aza-dR inhibitor does not mimic the geometric features of the planar oxacarbenium ion intermediate but, instead, may be capturing structural and electronic aspects of the subsequent transition state in which the glycosyl cation is presented to the attacking water. Additional evidence for this conclusion is presented below.

Electrostatically Induced Geometric Strain in 1-Aza-dR. The bond angles in the azafuranose ring are extremely

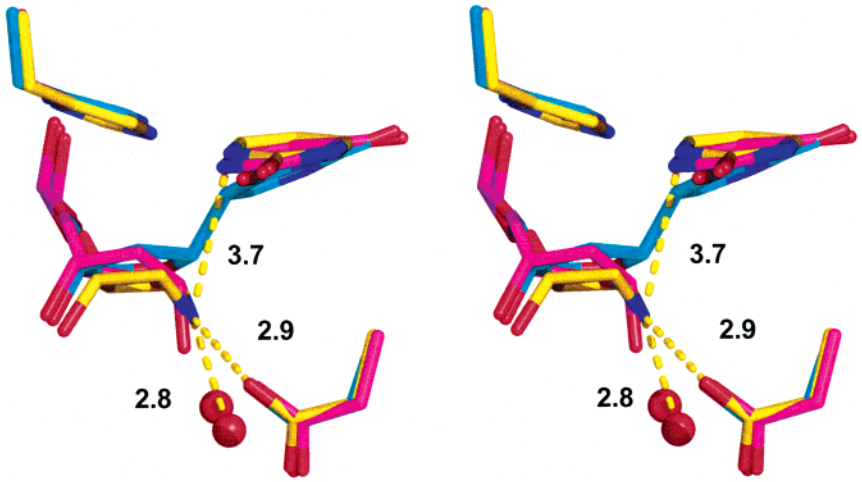

FIGURE 4: Structural alignment of the substrate, transition-state mimic, and product complexes of UDG. For the 1-aza-dR complex, key distances (in angstroms) between N1′ and the water nucleophile, uracil leaving group, and Asp145 are indicated.

distorted from their expected equilibrium geometries as determined using molecular mechanics calculations (Figure 3A,B), indicating extensive forces in the active site that give rise to this conformation. Most of the tetrahedral carbon atoms of the sugar ring show bond angles that are reduced from the predicted equilibrium geometries by as much as 10°, with the smallest angle observed for ∠C2′−N1′−C4′ = 97° (Figure 3A). The only enzyme groups that are poised to produce these distortions are Asp145 and the serine side chains and backbone atoms that rigidly hold the 3′- and 5′-phosphodiesters of the nucleotide (*18*). We were interested in whether immobilization of the DNA backbone or electrostatic interactions with Asp145 played a primary role in distorting the sugar, and we therefore performed a geometry optimization in which the C5′, C4′, C3′, and O3′ atoms were frozen to mimic the enzymatic forces that rigidly hold these atoms (Figure 3C). In this constrained analysis, the endocyclic angles of the carbon atoms were not found to be perturbed greatly from the unconstrained geometry optimization (Figure 3B), indicating that the unusual bond angles observed in the crystal model in Figure 3A likely arise from the electrostatic field provided by Asp145. Nevertheless, the rigid positioning of the phosphodiester backbone is certainly an important prerequisite that allows the highly localized flaplike motion of the anomeric center induced by Asp145.

Positioning and Electrostatic Guidance. Juxtaposition of the substrate, 1-aza-dR, and product complexes indicates that the 1′ position of the sugar migrates almost 1.5 Å to present itself to the attacking water and that nearly all of the substrate atoms are immobilized during the reaction course (Figure 4). A key observation from these structures is that the water nucleophile is unmoved between the substrate analogue and 1-aza-dR transition-state complexes (Figure 4). Since the previously characterized oxacarbenium ion intermediate has the same planar sugar ring conformation as the substrate (*14*), and given the nearly complete immobilization of the substrate and nucleophile across the entire reaction course (Figure 4), we infer that the water nucleophile must also be immobilized during the lifetime of the oxacarbenium ion intermediate. These structural observations are consistent with reaction coordinate movement of the electrophile but not the nucleophile. Accordingly, the rigidly planar oxacarbenium ion must be transformed into a bent conformation with carbonium ion character at C1′ to bring the electrophile and nucleophile into bonding distance ($r = 2.8$ Å; Figure 1). Given the high energy of localized carbonium ions as opposed to resonance-stabilized oxacarbenium ions (*23*, *24*), we propose that the observed structure mimics the ultimate transition state in which the attacking water is forming a nascent bond with C1′.

The above mechanism requires that the nucleophilic water be held in a fixed position by active site interactions until the moment the electrophile presents itself. Indeed, the water is splayed between two hydrogen bond acceptors: the side chain carboxylate oxygen of Asp145 and the N^{δ} ring nitrogen of His148, which is almost certainly in a neutral charge state to perform this role. These hydrogen bonds are fairly long (3.1 Å), which may facilitate escape of the water upon approach of the electrophile. As with the water nucleophile, these orienting groups are static throughout the reaction course, suggesting that a coupled network of interactions is involved in restricting the mobility of the reactive water. Careful positioning of the water is critical when such a highly reactive electrophile is generated in the active site; otherwise, adventitious nucleophiles may have an opportunity to attack, which could irreversibly inactivate the enzyme. In addition, electrostatic guidance of glycosyl cation migration is advantageous because it provides a mechanism to drive the reactive center away from the anionic uracil leaving group and toward the much weaker water nucleophile. We view this as a "bait-and-switch" mechanism in which the electrostatic field provided by the negatively charged aspartate lures the electrophile downward only to be captured by the bystander water.

Mapping the Reaction Coordinate. This new structure now allows a complete reconstruction of the structural transformations that occur in the UDG active site in the process of converting the substrate to products (Figure 5). The remarkable picture that emerges from these structures is that UDG manipulates the sugar conformation at each step along the reaction coordinate to facilitate catalysis. In the first step, binding energy is used to enforce a planar sugar conformation in the substrate that facilitates hyperconjugative stabilization of the dissociative transition state and oxacarbenium ion intermediate (*14*). In addition, binding energy is apparently used to reorient the uracil base into an unusual bent

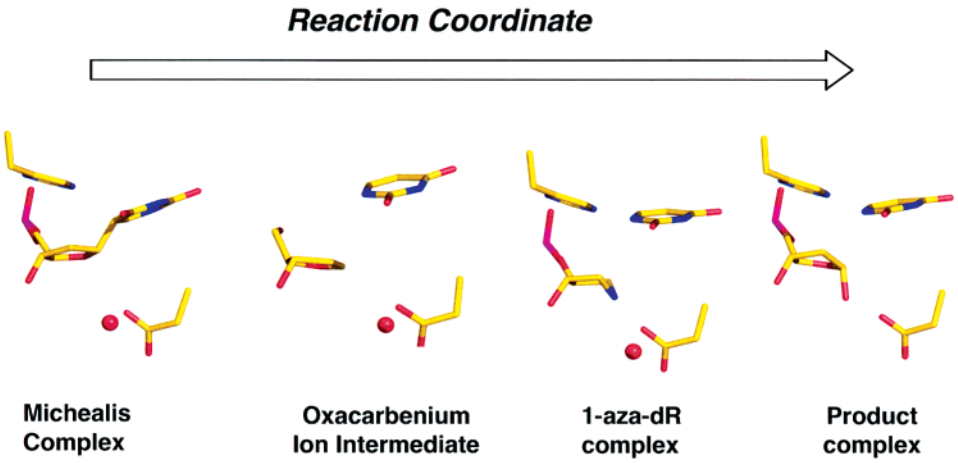

FIGURE 5: Structures along the reaction coordinate of UDG: the substrate complex with pseudodeoxyuridine (PDB code 1EMH), the model for the oxacarbenium ion intermediate derived from KIE measurements and the 1-aza-dR structure (*14*), the addition transition state determined from the complex of 1-aza-dR and uracil (PDB code 1Q3F), and the product complex of abasic DNA and uracil (PDB code 1SSP).

conformation that facilitates stereoelectronic control of electron flow from O4′ to the uracil leaving group (*4*, *25*). In the second transition state, electrostatic forces are used to pull the reactive electrophile 1.5 Å downward toward the poised water nucleophile. Taken together, this series of structures uncovers a another remarkable example of least nuclear motion and electrophile migration in glycosyl transfer (*15*, *26*) and extends the generality of this mechanism from retaining β-glycosidases (*27*) and purine nucleoside phosphorylase (*26*) to DNA repair glycosidases.

CONCLUSIONS

These results provide an example of how structural mimicry of a transition state can provide detailed mechanistic information about a reaction coordinate that is not readily obtained by other means. The electrophile migration mechanism of UDG, which only involves the reactive center itself, is an exquisite example of least atomic motion in enzymatic catalysis. Such a least motion mechanism for electrophile migration may be advantageous because the UDG active site is engineered to rigidly enforce sugar and phosphate conformations in the substrate complex that support formation of the planar oxacarbenium ion intermediate. Thus, movement of any sugar atoms other than C1′ in the second transition state would require disruption of these already established interactions and could contribute substantially to the reaction barrier in the final addition step. In general, cationic 1-azadeoxyribose inhibitors may best serve as mimics of addition transition states in which a nucleophile adds to a fully formed glycosyl cation intermediate. In contrast, the related 4-azadeoxyribose (*28*) may mimic the electronic properties of the sugar at an earlier point on the reaction pathway in which the positive charge is more localized on O4′.

REFERENCES

1. Schramm, V. L. (2001) *Curr. Opin. Chem. Biol. 5*, 556−564.
2. Zechel, D. L., and Withers, S. G. (2000) *Acc. Chem. Res. 33*, 11−18.
3. Parikh, S. S., Mol, C. D., Slupphaug, G., Bharati, S., Krokan, H. E., and Tainer, J. A. (1998) *EMBO J. 17*, 5214−5226.
4. Parikh, S. S., Walcher, G., Jones, G. D., Slupphaug, G., Krokan, H. E., Blackburn, G. M., and Tainer, J. A. (2000) *Proc. Natl. Acad. Sci. U.S.A. 97*, 5083−5088.
5. Drohat, A. C., and Stivers, J. T. (2000) *Biochemistry 39*, 11865−11875.
6. Drohat, A. C., and Stivers, J. T. (2000) *J. Am.Chem. Soc. 122*, 1840−1841.
7. Drohat, A. C., Xiao, G., Tordova, M., Jagadeesh, J., Pankiewicz, K. W., Watanabe, K. A., Gilliland, G. L., and Stivers, J. T. (1999) *Biochemistry 38*, 11876−11886.
8. Dong, J., Drohat, A. C., Stivers, J. T., Pankiewicz, K. W., and Carey, P. R. (2000) *Biochemistry 39*, 13241.
9. Werner, R. M., and Stivers, J. T. (2000) *Biochemistry 39*, 14054−14064.
10. Jiang, Y. L., Drohat, A. C., Ichikawa, Y., and Stivers, J. T. (2002) *Biochemistry 41*, 7116−7124.
11. Jiang, Y. L., Drohat, A. C., Ichikawa, Y., and Stivers, J. T. (2002) *J. Biol. Chem. 277*, 15385−15392.
12. Jiang, Y. L., and Stivers, J. T. (2003) *Biochemistry 42*, 1922−1929.
13. Dinner, A. R., Blackburn, G. M., and Karplus, M. (2001) *Nature 413*, 752−755.
14. Werner, R. M., and Stivers, J. T. (2000) *Biochemistry 39*, 14054−14064.
15. Schramm, V. L., and Shi, W. (2001) *Curr. Opin. Struct. Biol. 11*, 657−665.
16. Jiang, Y. L., Ichikawa, Y., Song, F., and Stivers, J. T. (2003) *Biochemistry 42*, 1922−1929.
17. Slupphaug, G., Eftedal, I., Kavli, B., Bharati, S., Helle, N. M., Haug, T., Levine, D. W., and Krokan, H. E. (1995) *Biochemistry 34*, 128−138.
18. Werner, R. M., Jiang, Y. L., Gordley, R. G., Jagadeesh, G. J., Ladner, J. E., Xiao, G., Tordova, M., Gilliland, G. L., and Stivers, J. T. (2000) *Biochemistry 39*, 12585−12594.
19. Otwinoski, Z., and Minor, W. (1997) *Methods Enzymol. 276*, 307−325.
20. Collaborative Computational Project, Number 4 (1994) *Acta Crystallogr. D50*, 760−776.
21. Jones, T. A., Zou, J. Y., Cowan, S. W., and Kjeldgaard, M. (1991) *Acta Crystallogr. A47*, 110−119.
22. Brunger, A. T., Adams, P. D., Clore, G. M., DeLano, W. L., Gros, P., Grosse-Kunstleve, R. W., Jiang, J. S., Kuszewski, J., Nilges, M., Pannu, N. S., Read, R. J., Rice, L. M., Simonson, T., and Warren, G. L. (1998) *Acta Crystallogr. D54*, 905−921.
23. Hehre, W. J. (1975) *Acc. Chem. Res. 8*, 369−376.
24. Forcasiu, D., and Horsley, J. (1980) *J. Am. Chem. Soc. 102*, 4906.
25. Stivers, J. T., and Jiang, Y. L. (2003) *Chem. Rev. 103*, 2729−2759.
26. Fedorov, A., Shi, W., Kicska, G., Fedorov, E., Tyler, P. C., Furneaux, R. H., Hanson, J. C., Gainsford, G. J., Larese, J. Z., Schramm, V. L., and Almo, S. C. (2001) *Biochemistry 40*, 853−860.

27. Vocadlo, D. J., Davies, G. J., Laine, R., and Withers, S. G. (2001) *Nature 412*, 835−838.
28. Scharer, O. D., Nash, H. M., Jiricny, J., Laval, J., and Verdine, G. L. (1998) *J. Biol. Chem. 273*, 8592−8597.
29. DeLano, W. L. (2002) The PyMOL Molecular Graphics System (http://www.pymol.org).

BI035372+